J Comput Aided Mol Des (2013) 27:257–276
DOI 10.1007/s10822-013-9638-6

Density functional and molecular docking studies towards investigating the role of single-wall carbon nanotubes as nanocarrier for loading and delivery of pyrazinamide antitubercular drug onto pncA protein

Nabanita Saikia · Sanchaita Rajkhowa · Ramesh C. Deka

Received: 27 September 2012 / Accepted: 4 February 2013 / Published online: 15 February 2013

Abstract The potential biomedical application of carbon nanotubes (CNTs) pertinent to drug delivery is highly manifested considering the remarkable electronic and structural properties exhibited by CNT. To simulate the interaction of nanomaterials with biomolecular systems, we have performed density functional calculations on the interaction of pyrazinamide (PZA) drug with functionalized single-wall CNT (*f*SWCNT) as a function of nanotube chirality and length using two different approaches of covalent functionalization, followed by docking simulation of *f*SWCNT with pncA protein. The functionalization of pristine SWCNT facilitates in enhancing the reactivity of the nanotubes and formation of such type of nanotube-drug conjugate is thermodynamically feasible. Docking studies predict the plausible binding mechanism and suggests that PZA loaded *f*SWCNT facilitates in the target specific binding of PZA within the protein following a lock and key mechanism. Interestingly, no major structural deformation in the protein was observed after binding with CNT and the interaction between ligand and receptor is mainly hydrophobic in nature. We anticipate that these findings may provide new routes towards the drug delivery mechanism by CNTs with long term practical implications in tuberculosis chemotherapy.

Keywords Carbon nanotubes · Functionalization · Density functional theory · Protein-nanotube interaction · Docking

Electronic supplementary material The online version of this article (doi:10.1007/s10822-013-9638-6) contains supplementary material, which is available to authorized users.

N. Saikia · S. Rajkhowa · R. C. Deka (✉)
Department of Chemical Sciences, Tezpur University, Napaam, Tezpur 784 028, Assam, India
e-mail: ramesh@tezu.ernet.in

Introduction

Drug delivery by nanomaterials is an active emergent research area and CNTs draws considerable potential application owing to its unique quasi one-dimensional structure and electronic properties [1]. SWCNTs have been selectively employed to deliver biologically active molecules across the cell membranes and facilitated by its nanodimension, high aspect (surface to volume) ratio, and structural stability, assists in the multiple loading of active cargos and probe molecules like fluorescein, plasmid DNA, proteins along with prolonged blood circulation time within the body [2–6]. The ability of CNTs to penetrate inside the cells of the body [7] without the need of any intracellular transport system [8] renders them suitable in biosensing application [9], tissue engineering [10] and biomedical devices [11]. As pristine CNTs are quite toxic due to their low solubility in most of the common organic and aqueous solvents along with their ability to self-aggregate (due to their high hydrophobicity); rendering the nanotubes biocompatible requires precise functionalization using covalent and noncovalent schemes [12–15]. Noncovalent functionalization basically involves electrostatic, hydrogen bonding, π–π stacking and van der Waals interaction [16, 17] whereas covalent functionalization incorporates the attachment of functional molecules onto the tube sidewall and edges by the formation of stable covalent bonds. Functionalization of CNTs with carboxylic acid remains the preferred choice for covalent functionalization as it proffers with the possibility of a variety of substitution reactions. Likewise, functionalization of nanotubes using 1,3-dipolar cycloaddition (1,3-DC) of azomethine ylide group is also a widely adopted method as it involves the formation of stable five membered ring onto the tube sidewall to which substitution and multiple attachment of functional moieties is achievable [18–21].

The covalent and noncovalent attachment of therapeutic molecules onto the sidewalls of CNTs have been widely studied with an envision to use CNTs as carrier payloads in target specific drug delivery applications [22–25]. Prato and co-workers [13] showed that functionalized nanotubes are quite biocompatible and nontoxic at the cellular level, offering potential application for drug administration within the body. Loading of anticancer drug molecules like cisplatin, doxorubicin (DOX), taxol, and methotrexate (MTX) onto nanotube sidewall has been studied for application in cancer chemotherapy [26] along with anti-inflammatory steroid dexamethasone [27] and antibacterial drug amphotericin [28]. Ali-Boucetta et al. [29] investigated the interaction of anticancer drug DOX with CNTs for effective drug delivery within the body. Pastorin et al. [30] adopted the functionalization of multi walled carbon nanotubes (MWCNTs) using 1,3-DC reaction for loading of MTX anticancer drug and fluorescent probe molecules. Fagan and co-workers [31] carried out theoretical studies on interaction of anti-inflammatory drug nimesulide with capped pristine and Si-doped CNTs. It is noteworthy to point here that the optimum length of the poly ethylene glycol (PEG) chain used for the covalent functionalization is essential as longer PEG chains can interfere with the drug administration within the body as it can block the interaction between the nanotube and cell lines of the body, cellular uptake of drug, and degrade the therapeutic function of the drug molecules [32]. The PEG functional units with superior hydrophilicity, biocompatibility and low immunogenicity can resist the opsonisation and increase the retention time of the nanotube-drug conjugate system in vivo [33, 34].

Just as treatment of cancer is the reason of global concern, Tuberculosis (TB) is another leading pathogen caused by the bacterium *Mycobacterium tuberculosis* with an estimated death rate of 2–3 million people and 8 million people getting infected per year [35]. Current therapy of TB consists of a combination of three chemotherapeutics namely: isoniazid (INH), PZA and rifampin (rifampicin) [36]. PZA is metabolized into its active form (pyrazoic acid) by the amidase activity of *M. tuberculosis* nicotinamidase/pyrazinamidase (MtPncA) encoded by the pncA gene [37–40]. Mutation in PZAse coding gene (pncA) causes significant loss in PZAse activity along with physiochemical alteration in the active metal binding (either iron or zinc) [41, 42]. Nevertheless, administration of PZA in high dosage can cause minor to detrimental health problems and the antibiotic resistance of bacteria under prolonged exposure triggers the need for better drug delivery methods to directly bind with the TB bacteria. Gallo et al. [43] investigated the role of armchair (5,5) SWCNT and fullerene as nanovectors for loading and delivery of INH antitubercular drug molecule. In our previous DFT study on the interaction of PZA drug with functionalized (5,5) armchair SWCNT [44], we established that CNTs favour the loading of PZA molecule onto its sidewall and covalent functionalization affects nanotubes structural and electronic properties. We also investigated the noncovalent functionalization of PZA onto armchair (5,5) and zigzag (9,0) SWCNTs wherein the modification of nanotube electronic properties upon π–π stacking interaction with PZA molecule have been discussed [45].

To elucidate the means of PZA drug delivery by SWCNTs onto active site of pncA protein, we carried out combined DFT and molecular docking studies on PZA loaded *f*SWCNT with wild type *M. tuberculosis* pncA enzyme. The docking of chemotherapeutic drug molecule onto the binding site of receptor and determining its binding affinity is an important parameter in modeling structure based drug delivery systems. We propose the two major schemes for the covalent functionalization: (1) sidewall functionalization using 1,3-DC reaction, and (2) edge functionalization using amidation reaction. Our results predict that the extent of interaction of PZA with (*n*,0) SWCNT is dependent on the length of the nanotube and its diameter. A comparison of HOMO–LUMO energy gap, global reactivity descriptor values along with frontier orbital analysis prior to and after functionalization in the close proximity of Fermi region have been discussed to contemplate the feasibility of covalent functionalization of SWCNTs. Following the DFT simulation, we performed docking studies on bare PZA and *f*SWCNT/PZA system with pncA for target specific delivery of PZA drug within the active binding site of pncA protein. We anticipate that these studies can provide a vivid understanding as to the role of SWCNTs in the recognition of specific target site within the protein thereby facilitating in the drug delivery prospects. In all the docking studies, conformational changes associated within the protein after docking were studied to investigate whether the nanotube imbibes any major structural deformation in the protein structure. Thus, in our study we present an interface between DFT, and molecular docking simulation to demonstrate the drug binding and its subsequent delivery by functionalized CNTs which can aid in structure based designing of novel drug delivery systems helpful in futuristic experimental studies in TB chemotherapy.

Computational details

In the quantum chemical calculations, the covalent functionalization of PZA onto zigzag (*n*,0) SWCNTs were modeled using two varied approaches for covalent functionalization widely used for experimental synthesis: one through 1,3-DC of azomethine ylide [46–48] and the other by amidation reaction [49] at the nanotube edges. PZA, pristine zigzag (*n*,0) SWCNT ($n = 9$, 10, 11 and 12) and the corresponding PZA/(*n*,0) SWCNT complexes were individually optimized in gas phase using DMol^3 program

[50]. Two length scales of nanotubes (one comprising of three unit cells and longer nanotubes comprising of five unit cells) with the ends terminated by hydrogen atoms to saturate dangling carbon bonds were considered for the simulation as a function of nanotube length, diameter and chirality. For the edge functionalization of (*n*,0) SWCNTs with substituted –COOH functional units, three model nanotubes namely; (9,0), (10,0) and (11,0) SWCNTs were considered each comprising of five unit cells. The two approaches of covalent functionalization facilitates in the incorporation of amino functional groups along the sidewall and tips of SWCNT rendering the nanotubes highly soluble in aqueous solvents mimicking the biological environment within the human body. Spin restricted calculations using the GGA/PW91 functional [51] and double numerical plus polarization (DNP) basis set which is equivalent to 6–31G** basis set of Gaussian were used in the calculations with all atoms relaxed during geometry optimization.

To evaluate the interaction of PZA molecule with *f*SWCNT, the binding energy was calculated using the following equations:

(a) 1,3-dipolar cycloaddition reaction

$$E_b = E_{(\mathrm{SWCNT/PZA})} - E_{(\mathrm{PEG-PZA\ chain})} - E_{(\mathrm{SWCNT})} \quad (1)$$

where $E_{(\mathrm{SWCNT/PZA})}$ is the total energy of *f*SWCNT loaded with PZA drug after full geometry optimization, $E_{(\mathrm{SWCNT})}$ is the energy of pristine zigzag SWCNT and $E_{(\mathrm{PEG\text{-}PZA\ chain})}$ is the total energy of the PEG chain bearing the drug molecule.

(b) Amidation reaction: The binding energy (B.E.) for the amidation reaction was calculated as follows: Energy of one CONH–PEG–PZA group formation at nanotube terminated initially with H atoms was calculated by considering a hypothetical reaction:

$$\mathrm{SWCNT-H} + \mathrm{CH_3CONH-PEG-PZA} \rightarrow \mathrm{SWCNT-CONH-PEG-PZA} + \mathrm{CH_4} \quad (2)$$

The B.E. was then determined by

$$E_\mathrm{b} = E_{(\mathrm{SWCNT-CONH-PEG-PZA})} + E_{(\mathrm{CH_4})} - E_{(\mathrm{SWCNT-H})} - E_{(\mathrm{CH_3CONH-PEG-PZA})} \quad (3)$$

A negative B.E. value implies thermodynamic favorability towards the covalent attachment of PZA drug onto the sidewall of zigzag (*n*,0) nanotube. The SCF tolerance is taken to be 1.0×10^6 and for plotting the volumetric properties like the frontier orbitals fine grid (0.15 Å grid intervals), border of 3.0 Å and contour plots having isovalue of 0.03 au were chosen to produce a higher quality grid.

From the optimized geometries, quantum molecular descriptors like global hardness (η), chemical potential (μ) derived using the Koopmans' theorem were calculated and compared. The quantum molecular descriptors like η and μ carry information about the global properties of the molecules like their structural stability and/or reactivity. The concept of electronegativity put forward by Pauling [52] is defined as "*the power of an atom in a molecule to attract electrons towards itself*". Higher is the electronegativity of the species, greater is its electron accepting power or rather the electrophilicity. On the other hand, the concept of hardness first formulated by Pearson [53, 54] states "*hard like hard and soft like soft*", and forms the basis of the popular hard soft acid base (HSAB) principle.

In an *N*-electron system having total energy (E) and external potential $\upsilon(\vec{r})$, the electronegativity (χ) is given by:

$$\chi = -\left(\frac{\delta E}{\delta N}\right)_{v(\vec{r})} = -\mu \quad (4)$$

where μ is defined as the negative of electronegativity. The η is expressed in terms of second derivative of energy with respect to the external potential $\upsilon(\vec{r})$ and is given by:

$$\eta = \frac{1}{2}\left(\frac{\delta^2 E}{\delta N^2}\right)_{v(\vec{r})} \quad (5)$$

According to Mulliken [55] the working equations for μ and η using the finite difference method are given by:

$$\mu = -\chi = -\frac{1}{2}(I + A) \quad (6)$$

and

$$\eta = \frac{1}{2}(I - A) \quad (7)$$

where I is the ionization potential and A the electron affinity of the molecule.

Molecular docking studies virtually predict the plausible binding mode based on various docking scoring functions and helps to understand how the nanocarrier and receptor plug into each other like that of a lock and a key. The molecular docking simulation provides an insight into (1) the characterization of binding cavity of the protein, (2) the orientation of the ligand with respect to receptor protein, and (3) the extent of interaction of the protein with functionalized SWCNT [56]. For the docking simulation, the crystal structure of pncA protein was retrieved from the protein data bank (PDB: 3PL1). The docking simulations were performed using Molegro Virtual Docker (MVD) [57] for active binding of SWCNT loaded PZA onto the protein. MolDock is based on a new hybrid search algorithm, called glided differential evolution which combines the differential evolution optimization technique with a cavity

prediction algorithm [58]. The docking score function is an extension of piecewise linear potential (PLP) [59] which includes the H-bonding and electrostatic terms and the re-rank scoring function identifies the most promising docking solution further increasing the docking accuracy. For each of the complexes we performed 100 independent runs with each of the runs returning one solution (pose) and in addition to the docking scoring function, terms like the sp^2–sp^2 torsion and Lennard-Jones 12-6 potential were also used [60]. The solutions were re-ranked and the highest ranked solution was taken as the best docked conformation with the protein. The re-ranking score function is computationally more expensive than the scoring function used during the docking simulation but it is generally yields better results than the docking score function in determining the best pose amongst the several poses originating from the same ligand [57]. The best docked conformation was selected on the basis of MolDock score and re-rank score values and visualized using Molegro Virtual Viewer and Chimera softwares. We performed docking simulations on bare PZA drug, PZA functionalized (n,0) SWCNTs via 1,3-DC and amidation reactions onto pncA protein for all the studied systems and modes of functionalization. Likewise, docking simulation on PZA encapsulated inside (n,0) SWCNTs (n = 10–12) for finite length nanotubes were studied. Multiple loading and subsequent delivery of PZA inside pncA protein were modeled onto two model nanotubes each comprising of five unit cells namely, armchair (6,6) and zigzag (10,0) SWCNT, which are the minimum diameters of nanotube suitable for encapsulation. We inserted two PZA drug molecules inside (6,6) and (10,0) SWCNTs and the PZA/SWCNT complexes were docked with the pncA protein. The population size, maximum interactions, scaling factor, and crossover rate were set to 150, 1,000, 0.50, and 0.90, respectively. Glided differential evolution and tripos force-field based docking scoring function were used to search for the binding orientation and conformation of each candidate molecule. Finally, ADMET (Absorption, Distribution, Metabolism, Excretion and Toxicity) properties were predicted with the help of the Pre-ADMET server (http://preadmet.bmdrc.org/) to discern whether our studied systems have the potential for any adverse effect in the human body upon administration.

Results and discussion

Covalent functionalization using 1,3-DC reaction

Structure and energetics

Figure 1 describes the optimized geometries of PZA, pristine (n,0) SWCNT and model nanotube depicting the covalent attachment of PZA onto SWCNTs through 1,3-DC functionalization at the tube sidewall. In pristine nanotubes, the average C–C bond length is calculated to be 1.42 Å which corresponds to the delocalized sp^2 hybridization. Upon functionalization (Fig. 1f), the C–C bond length stretches to 1.59 Å which corresponds to the partial re-hybridization from sp^2 to sp^3 at the site of covalent attachment, and this distortion influences nanotube electronic properties. Table 1 provides the values of B.E., Fermi energies, HOMO–LUMO energy gap, global parameters of PZA, pristine and PZA functionalized (n,0) SWCNTs for 3 unit cell nanotube systems and the pictorial depiction of the variation in B.E., HOMO–LUMO energy gap and global reactivity descriptors are shown in Fig. 2. From thermodynamic perspective, the B.E. values of PZA/(n,0) SWCNT complexes decreases with increase in nanotube diameter (Table 1) because nanotubes with large diameter have less curvature and the strain induced due to pyramidal angle is much lower compared to tubes with narrow diameter. The trend in variation of B.E. value suggests that in general, sidewall functionalization is viable on all the studied zigzag nanotubes (negative values of B.E.) and follows the generally accepted rule of sidewall

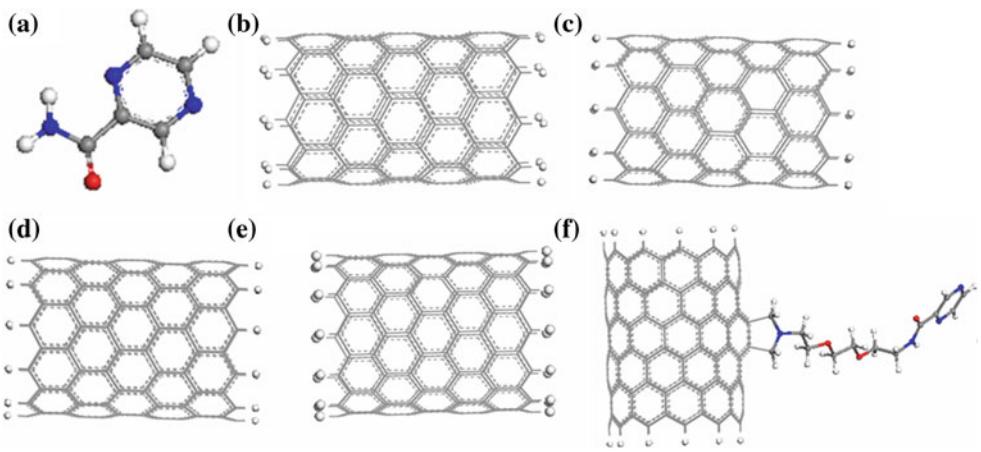

Fig. 1 Optimized geometries of **a** Pyrazinamide, pristine, **b** (9,0) SWCNT, **c** (10,0) SWCNT, **d** (11,0) SWCNT, **e** (12,0) SWCNT and **f** Model SWCNT depicting the site for covalent attachment of pyrazinamide molecule onto the nanotube sidewall

Table 1 The diameter (D, Å) of the studied SWCNTs, binding energy (E_b, eV), Fermi Energy (E_f, eV) HOMO, LUMO energies, HOMO–LUMO energy gap (eV) and global reactivity descriptors (η and μ, eV) of PZA, pristine and functionalized zigzag SWCNTs comprising of three unit cells

Molecule	D	E_b	E_f	HOMO	LUMO	HOMO–LUMO gap	$\eta = \frac{(I-A)}{2}$	$\mu = -\frac{(I+A)}{2}$
Pyrazinamide				−6.022	−3.216	2.806	1.403	−4.619
(9,0) SWCNT	7.05		−4.074	−4.581	−3.963	0.618	0.309	−4.272
PZA/(9,0) SWCNT		−1.133	−4.094	−4.306	−3.948	0.358	0.179	−4.127
(10,0) SWCNT	7.83		−4.085	−3.994	−3.905	0.089	0.044	−3.949
PZA/(10,0) SWCNT		−1.018	−4.026	−3.969	−3.934	0.035	0.017	−3.951
(11,0) SWCNT	8.61		−4.101	−3.992	−3.633	0.359	0.179	−3.812
PZA/(11,0) SWCNT		−0.859	−4.103	−3.972	−3.698	0.274	0.137	−3.835
(12,0) SWCNT	9.39		−4.116	−4.020	−3.979	0.041	0.020	−3.999
PZA/(12,0) SWCNT		−0.713	−4.059	−3.978	−3.941	0.037	0.018	−3.959

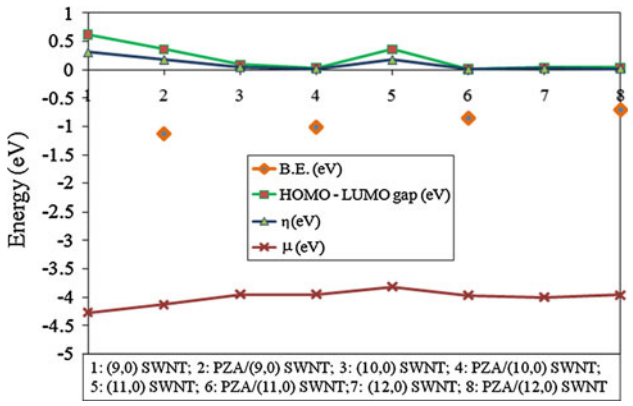

Fig. 2 The variation of binding energy (eV), HOMO–LUMO energy gap (eV), global hardness (η) and chemical potential (μ) of pristine and functionalized zigzag (n,0) nanotubes comprising of three unit cells

reactivity of SWCNTs i.e. larger the diameter of the nanotube low is its exothermicity towards 1,3-DC reaction [61]. Nanotubes with narrow diameter demonstrate more negative B.E. values and covalent attachment of functional moieties onto the narrow diameter tubes are thermodynamically more favoured than nanotubes with larger diameter. The trend in increasing nanotube reactivity with diameter has also been validated in the theoretical study by Lu et al. [61]. To correlate the results observed for finite length nanotubes, we extended the study to longer nanotubes (5 unit cells) to represent correctly the edge states applicable for realistic interpretation. We consider (9,0), (10,0) and (11,0) SWCNTs each comprising of 5 unit cells to study the interaction with PZA molecule, for both sidewall and edge functionalization as depicted in Fig. 3 for (9,0) SWCNT system and Supporting Information, Figures S1–S2 for (10,0) and (11,0) SWCNT systems, respectively. The (12,0) SWCNT/PZA system is not covered in this study because of computational limitation in handling such big nanotubes. The B.E. value (Table 2) decreases with increase in the nanotube diameter; a trend similar to that observed for 3 unit cell nanotubes although the values are comparatively lower in case of nanotubes comprising of 5 unit cells. This suggests that the model 3 unit cell nanotubes taken for the study can provide reasonable interpretation towards the variation in B.E. values. Since DFT GGA methodology underestimates the B.E. values [62], accordingly in realistic systems, binding energy values will be higher than the calculated parameters.

Global reactivity descriptors

The trend in variation of global reactivity descriptors for pristine (*n,0*) SWCNTs show that on an average with increase in nanotube diameter, HOMO–LUMO energy gap and η values gradually decreases except for (11,0) SWCNT system in which case the HOMO–LUMO energy gap and η values are higher than (10,0) and (12,0) SWCNTs but lower than (9,0) SWCNT (Fig. 2; Table 1). Compared to (5,5) SWCNT which has a diameter of 6.78 Å; (9,0) SWCNT has almost similar diameter of 7.15 Å. For perfect (*n*,0) SWCNTs (both 3 and 5 unit cells), the HOMO–LUMO energy gap and η value decreases with increase in nanotube diameter suggesting an increase in reactivity (lowering in stability) of the nanotubes with increase in tube diameter. Likewise, for the nanotubes with the same chirality but of a longer length, the HOMO–LUMO energy band gap decreases with increase in the length of the nanotubes (Tables 2) suggesting that length of nanotube plays a key determining role in the stability (reactivity). The observed trend in the variation of energy band gap for zigzag nanotubes have been investigated by Lukovits and co-workers [63] wherein they showed that, in general, armchair nanotubes are less reactive compared to zigzag nanotubes and the band gap decreases with increase in the length of the tubes. Unlike armchair nanotubes, where the

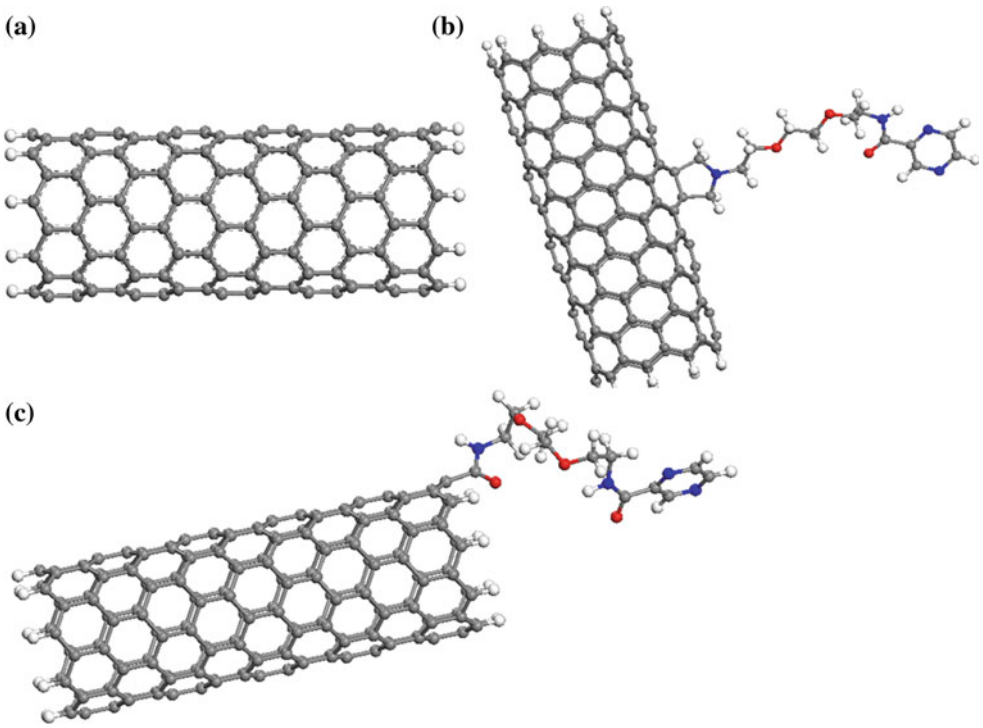

Fig. 3 The optimized geometries of **a** pristine (9,0) SWCNT comprising of 5 unit cells, **b** sidewall functionalized PZA/(9,0) SWCNT, **c** edge functionalized PZA/(9,0) SWCNT

Table 2 The binding energy (E_b, eV), Fermi Energy (E_f, eV), HOMO, LUMO energies, HOMO–LUMO energy gap (eV) and global reactivity descriptors [η (eV) and μ (eV)] of PZA, pristine and functionalized zigzag SWCNTs comprising of five unit cells

Molecule	E_b	E_f	HOMO	LUMO	HOMO–LUMO	$\eta = \frac{(I-A)}{2}$	$\mu = -\frac{(I+A)}{2}$
(9,0) SWCNT		−4.036	−4.420	−4.035	0.385	0.192	−4.227
PZA/(9,0) SWCNT (sidewall)	−1.120	−4.008	−4.197	−3.998	0.199	0.099	−4.097
PZA/(9,0) SWCNT (edge)	−0.075	−4.012	−4.040	−4.010	0.030	0.015	−4.025
(10,0) SWCNT		−3.985	−4.007	−3.935	0.072	0.036	−3.971
PZA/(10,0) SWCNT (sidewall)	−1.077	−4.007	−4.034	−3.985	0.049	0.024	−4.009
PZA/(10,0) SWCNT (edge)	−0.549	−4.107	−4.128	−4.084	0.044	0.022	−4.106
(11,0) SWCNT		−4.061	−4.056	−3.909	0.147	0.073	−3.982
PZA/(11,0) SWCNT (sidewall)	−0.780	−4.027	−4.003	−3.962	0.041	0.020	−3.982
PZA/(11,0) SWCNT (edge)	−0.244	−4.120	−4.099	−4.085	0.014	0.007	−4.092

HOMO–LUMO energy gap (reactivity) is related to the electronic states which remain delocalized throughout the nanotube sidewall, in zigzag (n,0) SWCNTs, the energy band gap basically resembles the edge states. The Fermi energy value increases with increase in nanotube diameter (except for 5 unit cell (10,0) SWCNT) indicating an increase in overall reactivity of the nanotubes and in turn affecting the energy gap and subsequently the nanotube electronic properties.

For the corresponding functionalized nanosystems, the HOMO–LUMO energy gap decreases for PZA/(n,0) SWCNT system compared to perfect SWCNTs which illustrates that functionalization and subsequent loading of PZA increases the reactivity of pristine nanotubes. The η value decreases with functionalization which also suggests the increase in reactivity of pristine nanotube after covalent attachment of functional units. The variation in μ values of pristine nanotubes (comprising of 3 unit cells) prior to and after functionalization is not very uniform as observed from Table 1 and Fig. 2. Physically, μ values describe the escaping tendency of electrons for a system under equilibrium conditions. The greater the μ value less stable (more reactive) is the species. Pristine (9,0) SWCNT has the lowest μ value, and with increase in the diameter of the nanotubes the μ value increases and then finally decreases for (12,0) SWCNT system (Fig. 2) which indicates the increase in reactivity of the nanotube with increasing diameter. Upon functionalization with PZA, for (9,0) and (12,0) SWCNT systems, the μ value increases whereas for (10,0) and (11,0) SWCNTs, the trend is the reverse and μ

value decreases with functionalization. The variation in μ values do not a regular trend for the studied nanotube systems upon 1,3-DC functionalization with PZA. Thus, a comparison of the HOMO–LUMO energy gap and global reactivity descriptors for the studied nanotube systems both prior to and after functionalization helps in understanding the structural stability/reactivity as well as the variation in electronic properties of the pristine nanotubes after 1,3-DC functionalization. The reactivity of the pristine nanotube varies as a function of the tube diameter and covalent functionalization further enhances the reactivity of the pristine nanotubes as it breaks the symmetry at the site of attachment of the functional moiety forming stable covalent bonds with the nanotube sidewall. In general for zigzag nanotubes, the edge states contribute towards the reactivity of the nanotube and electronic states are more predominant along tube edges rather than being delocalized on the sidewall which is further confirmed from the frontier orbital analysis discussed in the subsequent section.

Frontier orbital analysis

The computed electron density maps with isosurface of 0.03 au corresponding to the HOMO and LUMO of PZA and pristine (*n*,0) nanotubes are shown in Fig. 4. In PZA, HOMO (Fig. 4a) is delocalized around the aromatic pyrazine ring with major contribution from the electronegative oxygen atom and LUMO (Fig. 4b) has greater contribution on the carbon atoms. Except for (9,0) SWCNT, in rest of the (*n,0*) SWCNTs ($n = 10, 11, 12$) HOMO (Fig. 4e, g, i) and LUMO (Fig. 4f, h, j) orbitals are mainly localized along the nanotube edges rather than the sidewall except in (11,0) SWCNT where it is partially localized throughout the tube sidewall (Fig. 4h). This suggests that zigzag nanotubes are reactive at the edges with electronic charge density being localized along the edge carbon atoms rather than on the sidewall. The same trend in the distribution of electronic states towards the HOMO and LUMO is observed when we extend the study for the 5 unit cell nanotubes (Fig. 5 and Supporting Information, Figure S3). The (9,0) SWCNT although being a zigzag nanotube shows anomaly in the electronic distribution corresponding to the HOMO for 3 unit cells (Fig. 4c) and 5 unit cells (Fig. 5a, b), as (9,0) SWCNT being metallic in nature (n − m is a multiple of 3) the observed electronic states are similar to that of the metallic (5,5) SWCNT. The distribution of HOMO with the variation of nanotube diameter is manifested from the fact that with increase in tube diameter, electron density contributing from the HOMO is localized along nanotube edges with no distribution on the sidewalls. Thus, for (*n,0*) SWCNTs comprising of 5 unit cells, the HOMO (Fig. 5) and LUMO (Supporting Information, Figure S3) isosurface exhibits a similar trend in the frontier orbital distribution to that of the 3 unit cell nanotubes which signify that length of the nanotubes does not affect the behaviour of the charge localization/delocalization

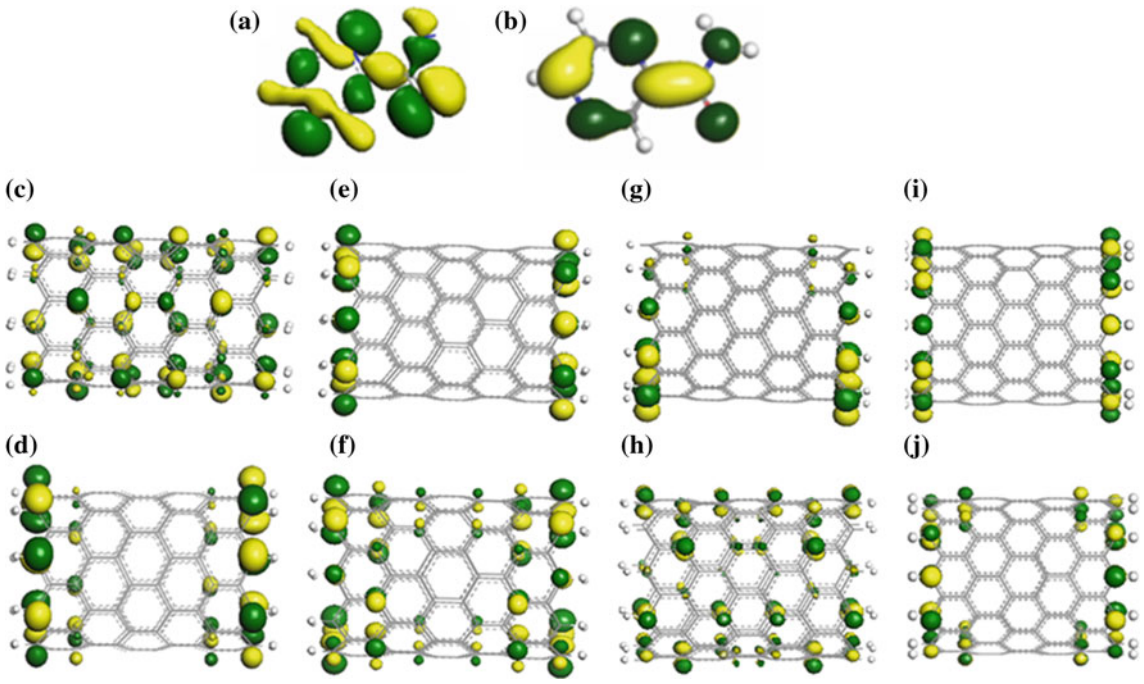

Fig. 4 The pictorial depicting of **a** HOMO in PZA drug, **b** LUMO of bare PZA drug, **c** HOMO of (9,0) SWCNT, **d** LUMO of (9,0) SWCNT, **e** HOMO of (10,0) SWCNT, **f** LUMO of (10,0) SWCNT, **g** HOMO of (11,0) SWCNT, **h** LUMO of (11,0) SWCNT, **i** HOMO of (12,0) SWCNT, **j** LUMO of (12,0) SWCNT

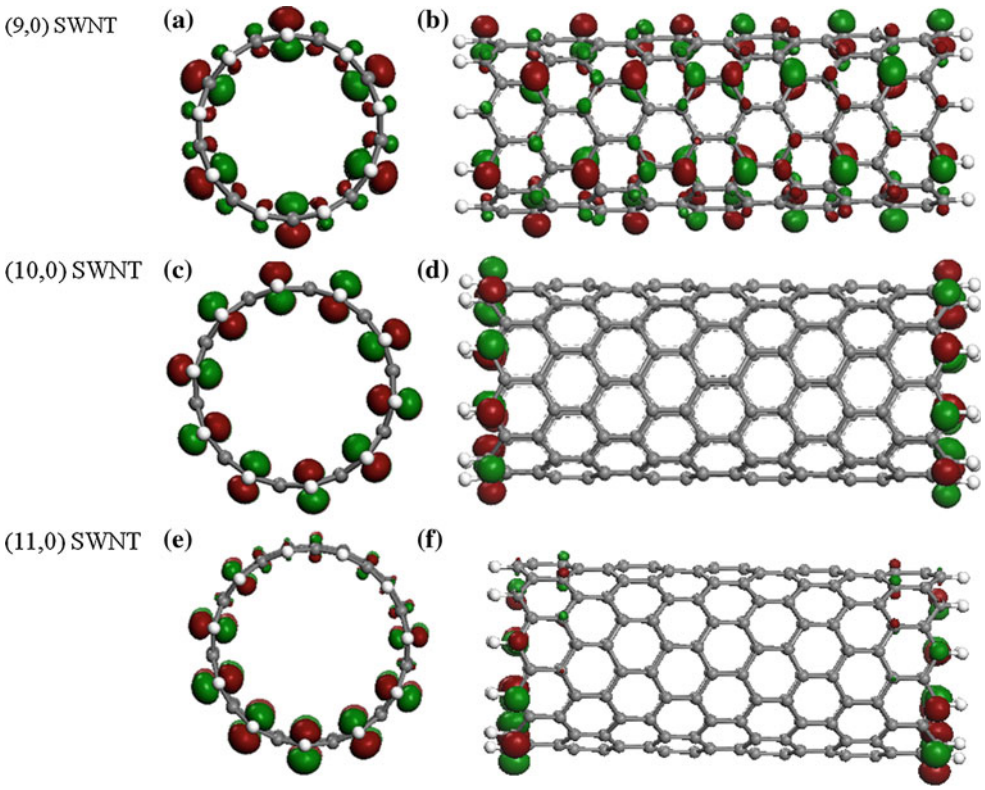

Fig. 5 The front and side view depiction of HOMO plots in pristine (9,0) SWCNT (**a**, **b**), pristine (10,0) SWCNT (**c**, **d**), pristine (11,0) SWCNT (**e**, **f**) each comprising of 5 unit cells

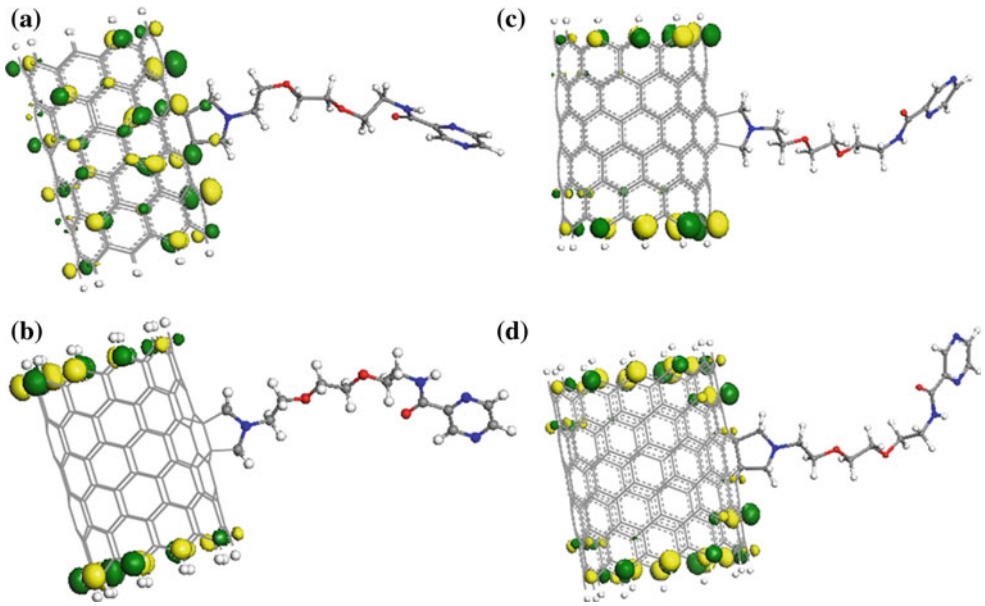

Fig. 6 The HOMO isosurface of **a** PZA/(9,0) SWCNT, **b** PZA/(10,0) SWCNT, **c** PZA/(11,0) SWCNT and **d** PZA/(12,0) SWCNT. The isosurface value is taken as 0.03 au

(reactivity of the edge states) of the nanotubes and in general for zigzag nanotubes (except for (9,0) SWCNT system) the frontier orbitals are mainly localized along the tube edges.

The HOMO and LUMO plots of sidewall functionalized PZA/(*n*,0) SWCNT (3 unit cells) are illustrated in Fig. 6 and Supporting Information Figure S4, the HOMO plots for PZA functionalized (9,0) SWCNT and (10,0) SWCNT systems each comprising of 5 unit cells are depicted in Fig. 7 and for PZA/(11,0) SWCNT system the HUMO isosurface is illustrated in Fig. 8a, b. The corresponding LUMO plots for sidewall functionalized PZA/(9,0) SWCNT and PZA/(10,0) SWCNT systems are provided in the Supporting Information, Figure S5 and for PZA/(11,0) SWCNT system the corresponding LUMO isosurface is depicted in Supporting information, Figure S6. Significant

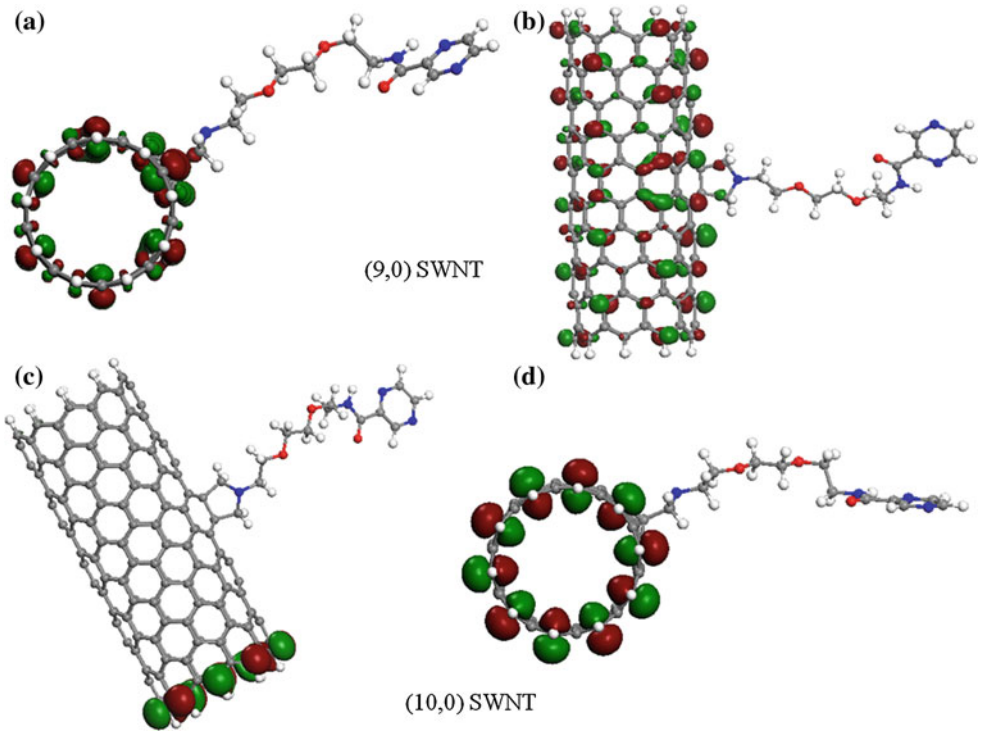

Fig. 7 The HOMO isosurface of **a** side view and **b** front view depiction of sidewall functionalized PZA/(9,0) SWCNT, **c** side view and **d** front view depiction of sidewall functionalized PZA/(10,0) SWCNT

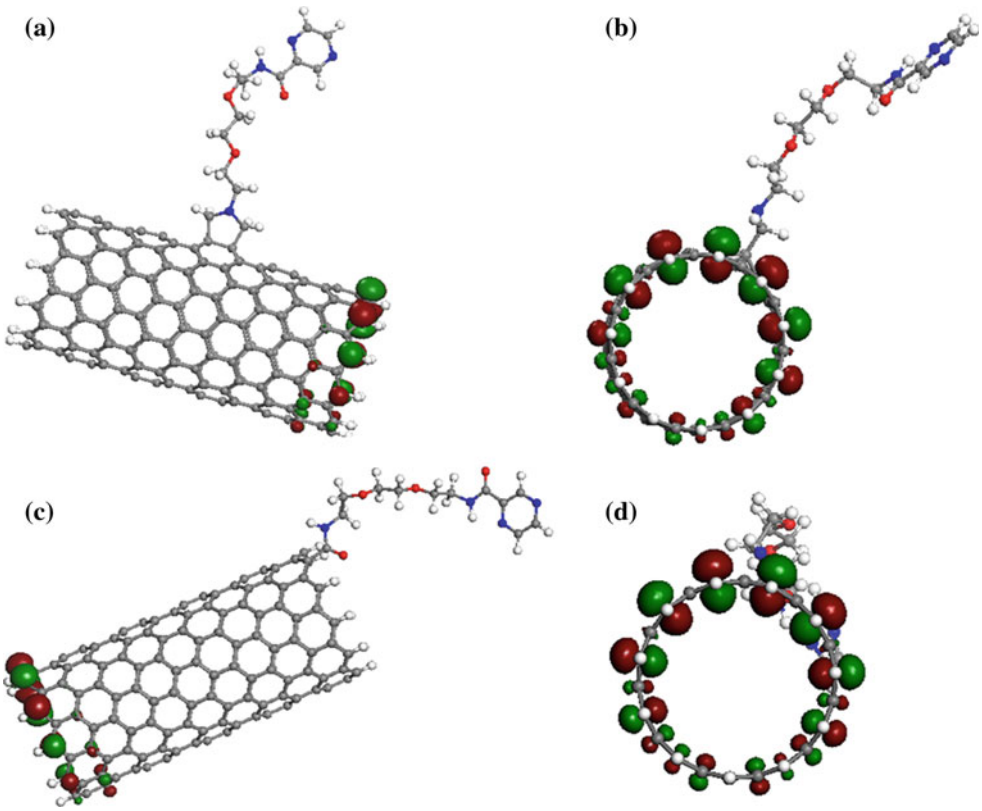

Fig. 8 **a** The side view, **b** front view depiction of the HOMO isosurface in sidewall functionalized PZA/(11,0) SWCNT, **c** side view, **d** front view depiction of HOMO in edge functionalized PZA/(11,0) SWCNT system

alteration in the HOMO isosurface of pristine (9,0) SWCNT is observed upon functionalization (Fig. 6a) and the electronic states get delocalized at the site of covalent attachment suggesting charge transfer between the C–C bond of nanotube and azomethine ylide functional unit, whereas the LUMO remains localized basically along the nanotube edges (Supporting information, Figure S4a). The charge transfer between C–C bond of nanotube and

azomethine ylide functional unit was confirmed with the help of Mulliken charge population analysis on pristine and sidewall functionalized (9,0) SWCNT system. Prior to functionalization, the Mulliken atomic charge on C161 and C156 atoms were calculated to be 0.002 |e| and −0.002 |e|, respectively. Upon covalent attachment of azomethine ylide at C161 and C156 atoms, the Mulliken atomic charge was calculated to be −0.224 |e| and −0.223 |e|, respectively. Covalent functionalization therefore results in significant charge transfer of around 0.226 |e| signifying strong interactions and perturbation of electronic states at the site of covalent attachment. For the other studied nanotubes, functionalization does not perturb the electronic states, which remain localized along the tube edges similar to that observed for pristine nanotubes. Interestingly, in PZA/(11,0) SWCNT system, LUMO of pristine (11,0) SWCNT (Fig. 4h) which initially remains delocalized throughout the nanotube sidewall, upon functionalization gets localized along the nanotube edges rather than the sidewall (Supporting information, Figure S4c), which is not observed in case of the other studied SWCNT systems. This shows that covalent functionalization of PZA onto (11,0) SWCNT affects the electronic properties of pristine (11,0) SWCNT by localizing the electronic charge density towards the tube edges rather than the sidewall.

In the case of 5 unit cell (*n*,0) SWCNT systems, for sidewall functionalized (9,0) SWCNT, the HOMO isosurface shows the reorientation of frontier orbitals around the C–C bonds bearing the functional moiety with charge localization on the azomethine ylide group and the adjoining aromatic benzenoid rings of the nanotube (Fig. 7a, b) whereas the LUMO isosurface remains delocalized along the tube edges with no contribution on the sidewall (Supporting Information, Figure S5a, b). In case of PZA/(10,0) SWCNT, sidewall functionalization demonstrates the electronic states corresponding to the HOMO to remain localized along one of the nanotube edges (Fig. 7c, d) with no contribution along the other end and the LUMO to be localized along the edges and the adjoining benzenoid rings of the tube close to the functional moiety (Supporting Information, Figure S5c and d). For PZA/(11,0) SWCNT system, the HOMO (Fig. 8a, b) isosurface basically remains localized along one of the nanotube edges with no contribution at the other end whereas the LUMO isosurface gets delocalized throughout the nanotube sidewall similar to the LUMO of pristine (11,0) SWCNT but with localized charge density on the azomethine ylide functional unit and the neighbouring carbon atoms (Supporting Information, Figure S6a, b). This trend depicts that sidewall attachment of functional units to an extent effects the electronic states of the pristine (11,0) nanotube as observed from the LUMO isosurface plots for both 3 unit cell and 5 unit cells.

Furthermore, HOMO − n and LUMO + n plots of both pristine and functionalized (*n*,0) SWCNT systems (Supporting Information, Figures S7–S10) shows that in pristine (9,0) SWCNT system, LUMO + 3 (Supporting Information, Figure S7a) and LUMO + 4 (Supporting Information, Figure S7b) isosurface remain localized along the tube edges, and for functionalized PZA/(9,0) SWCNT, LUMO + 3 orbital remains mostly delocalized along the edges (Supporting Information, Figure S7c) and LUMO + 5 orbital remains localized at the site of functionalization (Supporting Information, Figure S7d) with significant charge localization between (9,0) SWNT and PEG-PZA unit. In pristine (10,0) SWCNT the HOMO − 4 (Supporting Information, Figure S8a) and LUMO + 4 (Supporting Information, Figure S8b) orbitals get delocalized throughout the nanotube sidewall. Likewise for functionalized PZA/(10,0) SWCNT, HOMO − 3 (Figure S8c) as well as LUMO + 3 orbitals (Figure S8d) show prominent localization along the functionalized PEG unit with almost negligible contribution on edge C atoms. A similar phenomenon is observed in case of pristine and functionalized PZA/(11,0) SWCNT system (Supporting Information, Figure S9). Finally in (12,0) SWCNT system (Figure S10) the HOMO − 4 orbitals (Figure S10a) remain delocalized along the central ring of the nanotube with no contribution on the edges whereas LUMO + 4 orbitals get delocalized along the tube sidewall (Supporting Information, Figure S10b). After functionalization if we observe the HOMO − 3 and LUMO + 3 orbitals we see that the electronic states are more predominant at the sites where covalent attachment has taken place (Supporting Information, Figure S10c, d). This illustrates that in addition to the HOMO and LUMO frontier orbitals, the HOMO − n and LUMO + n orbitals help in providing a qualitative depiction to the charge localization/delocalization within the SWCNTs prior to and after functionalization and assists in understanding the modification in nanotube electronic properties.

Covalent functionalization of SWCNT using carboxylic acid

Structure and energetics

Figure 3c depicts the optimized geometries of edge functionalized (9,0) SWCNT and for (10,0) and (11,0) SWCNT systems, the optimized geometries are depicted in Supporting Information, Figures S1c and S2c. The C–C bond length at the site of covalent attachment onto the nanotube sidewall is calculated to be 1.488 Å. Unlike the sidewall functionalization of SWCNT with PEG, edge functionalization results in the PEG chain to lie in a twisted conformation which is quite interesting. Stability wise, edge

functionalization results in lower values of binding energy compared to sidewall functionalization for nanotubes of same chirality (Table 2). This can be understood from the fact that sidewall functionalization using 1,3-DC reaction forms a stable five-membered azomethine ring with the nanotube sidewall. On the other hand, for amidation functionalization, a simple substitution reaction mechanism is followed at one of the edge C–H bond which results in slight deformation in overall nanotube structural conformation, and thereby from thermodynamic stability perspective, edge functionalization is more facile compared to sidewall functionalization. With the increase in nanotube diameter, the binding energy value increases (tends towards more negative values), which is quite opposite to the trend observed for sidewall functionalization using 1,3-DC reaction. A proposed justification towards this trend in variation of binding energy value may be that nanotubes with higher diameter are under less strain compared to narrow diameter tubes and offer greater flexibility to the –CONHPEG side chain compared to sidewall functionalization and the exothermicity solely depends on the curvature induced stabilization of functional unit. Nevertheless, it can be said that both the studied modes of functionalization of SWCNTs are thermodynamically favoured and adsorption of PZA onto (*n*,0) SWCNTs is dependent on the chirality and length of the nanotubes along with the fact that 1,3-DC functionalization is thermodynamically, the better favoured mode of functionalization for drug delivery application.

Global reactivity descriptors

Table 2 summarizes the HOMO–LUMO energy gap and global reactivity descriptor values for edge functionalized (*n*,0) SWCNT systems. For edge functionalized PZA/(n,0) SWCNT, the variation in energy gap, η and μ values summarized in Table 2, illustrate that with increase in nanotube diameter the energy gap, η and μ value initially increases on moving from (9,0) SWCNT to (10,0) SWCNT and then decreases for (11,0) SWCNT system which illustrates that chirality of nanotube plays a significant role in nanotube reactivity. In general, with increase in nanotube diameter the energy gap and η value decreases and the calculated values are lower compared to sidewall functionalized nanotube which shows that edge functionalized nanotubes are more reactive compared to sidewall functionalized tubes. Except for (9,0) SWCNT/PZA system, the μ value increases with functionalization of the nanotubes. The global reactivity descriptor values for edge functionalized PZA/(n,0) SWCNT are much lower compared to sidewall functionalized counterparts which demonstrates that sidewall functionalization is more preferred from the thermodynamic perspective than edge functionalization.

Frontier orbital analysis

Figures 8 and 9 depict the front and side views of HOMO plots of edge functionalized (*n*,0) SWCNTs ($n = 9, 10, 11$) and the corresponding LUMO plots are provided in Supporting Information, Figures S6 for (11,0) SWCNT and S11 for (9,0) and (10,0) SWCNT systems, respectively. In PZA/(9,0) SWCNT, the HOMO (Fig. 9a, b) is delocalized along one of the tube edges bearing the functional unit illustrating charge transfer between PEG chain and C atoms of the tube. Similar to the 1,3-DC functionalization, the charge transfer between PEG chain and terminal C65 atom of the (9,0) nanotube was confirmed with the help of Mulliken charge population analysis. Prior to functionalization, the Mulliken atomic charge on C65 atom of pristine (9,0) SWCNT was calculated to be 0.002 |e|. Upon covalent attachment at C65 atom, the Mulliken atomic charge was calculated to be −0.095 |e|. Amidation functionalization therefore results in the charge transfer of around 0.097 |e| between the interacting groups which is lower by 0.129 |e| as observed in case of 1,3-DC functionalization. This suggests that compared to amidation functionalization, sidewall functionalization is quite stable with significantly higher charge transfer between the tube sidewall and the functional unit. The LUMO on the other hand is delocalized on the opposite edge of the nanotube (Supporting Information, Figure S11a, b). However, both HOMO and LUMO isosurface for amidation functionalized nanotubes show the edge states bearing the functional group to be reactive which is quite different from the frontier orbital distribution in sidewall 1,3-DC functionalized PZA/(9,0) SWCNT. For edge functionalized PZA/(10,0) SWCNT, HOMO remains delocalized on the opposite edge of nanotube (Fig. 9c, d) whereas the LUMO is distributed along the end of nanotube bearing the functional moiety (Supporting Information, Figures S11c, d). For PZA/(11,0) SWCNT system, the HOMO is basically delocalized at one of the nanotube edge (Fig. 8c, d) and LUMO remains delocalized along the edge of (11,0) SWCNT bearing the functional unit (Supporting Information, Figure S6c and d). Thus, in general we can say that unlike the sidewall functionalization, amidation reaction of (*n*,*0*) SWCNT results in electronic charge density to remain localized along the tube edges rather than the sidewall. As opposed to the frontier orbital distribution observed in PZA/(9,0) SWCNT and PZA/(11,0) SWCNT systems for 1,3-DC functionalization, which remain delocalized along the tube sidewall for amidation functionalization, the contribution to the electronic states is solely from the edge carbon atoms of the nanotube, which is quite an interesting observation. We can generalize that both the adopted modes of functionalization perturbs the electronic properties of the nanotubes in their respective ways, sidewall

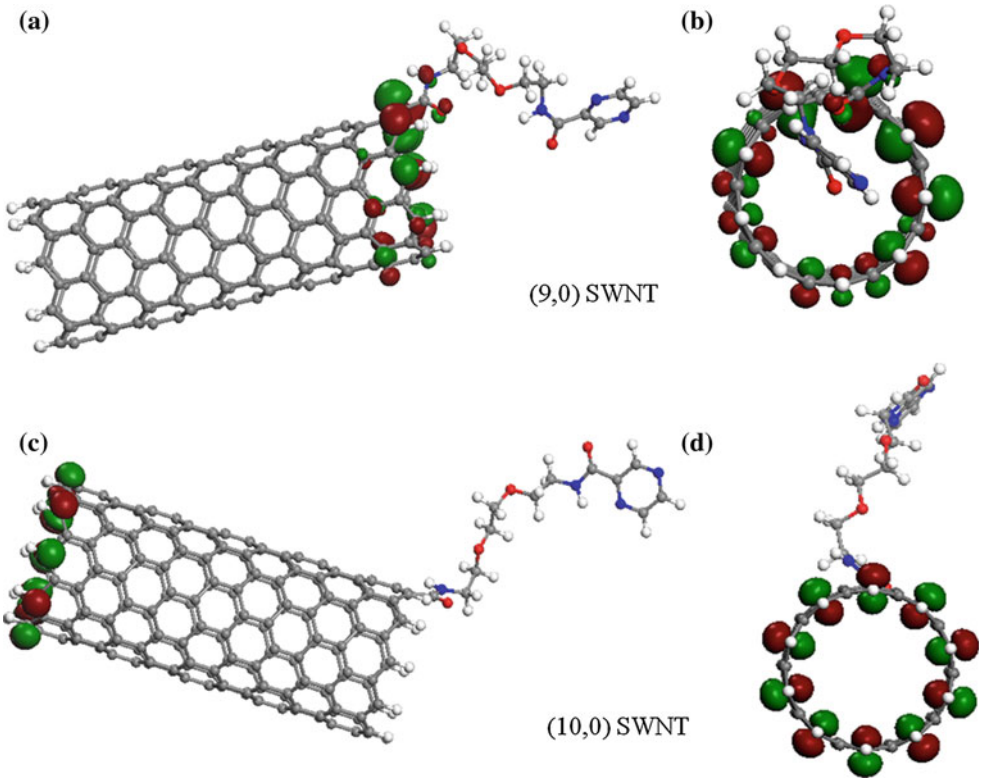

Fig. 9 The HOMO isosurface of **a** side view and **b** front view depiction of edge functionalized PZA/(9,0) SWCNT, **c** side view and **d** front view depiction of edge functionalized PZA/(10,0) SWCNT

functionalization alters the structural and electronic properties along the tube sidewall whereas edge functionalization affects the terminal carbon bonds without drastically distorting nanotube structure.

Docking of PZA functionalized (n,0) SWCNT with pncA protein

Crystal structure of pncA

Scorpio and Zhang in 1996 identified the PZase gene (*pncA*) from *M. tuberculosis* and showed the mutation in *pncA* to be the major mechanism towards PZA resistance [64, 65]. The crystal structure of pyrazinamidase pncA enzyme comprises of a six stranded parallel beta sheet with the helices packed on either side to form the α/β domain as illustrated in Fig. 10a. The active binding sites His51, His57, His71and Cys138 are labelled in closest proximity to the binding pocket for PZA interaction. The N-terminal unit of helix α3 bears the active cysteine residue of pncA i.e. Cys138. The co-factor present in pncA is Fe^{2+} (shown in brown colour of Fig. 10a) which is identified by the ICP-MS analysis to have a Fe^{2+} concentration of 260 μM in the protein assay [37]. The Fe^{2+} ion is coordinated to His51, His71 residues, HOH220, and HOH221 water molecules forming a tetragonal bipyramidal structure with the H_2O molecules lying at the equatorial position (depicted by red dots) and the side chain residues of Asp49 and His57 occupying the axial positions. Previous studies show that the mutation in pncA protein basically occurs as: His51Ala, His57Asp, and Asp49Gly for Fe^{2+} binding, Asp8, Lys96, and Cys138Ala for catalytic site and Phe13Leu, Trp68Leu for PZA binding within the pncA [66]. Various possibilities for docking of *f*SWCNT loaded PZA onto the pncA protein are investigated

(1) 1,3-DC functionalization of (*n,0*) SWCNT with PEG conjugated to PZA drug,
(2) Edge functionalization using amidation reaction, and
(3) Encapsulation of mono and multiple PZA drugs inside (*n,0*) and (*n,n*) SWCNTs

Docking simulation on covalently functionalized PZA/(n,0) SWCNTs. Bare PZA binding onto the active site of pncA is represented in Fig. 10b with the active amino acids in close proximity to PZA being labelled in the figure. A close depiction of the interaction of bare PZA drug with the amino acid residues of pncA protein can be observed from Fig. 10c, d which shows the hydrogen bonding of PZA with two of the active amino acids His71 and Asp49 at an optimum interacting distance of 3.02 and 3.24 Å, respectively (interaction shown in blue lines) which occurs through the amine group of PZA. PZA drug interacts electrostatically with the proximate amino acid Ala134 at an optimum distance of 2.55 Å (interaction shown in green

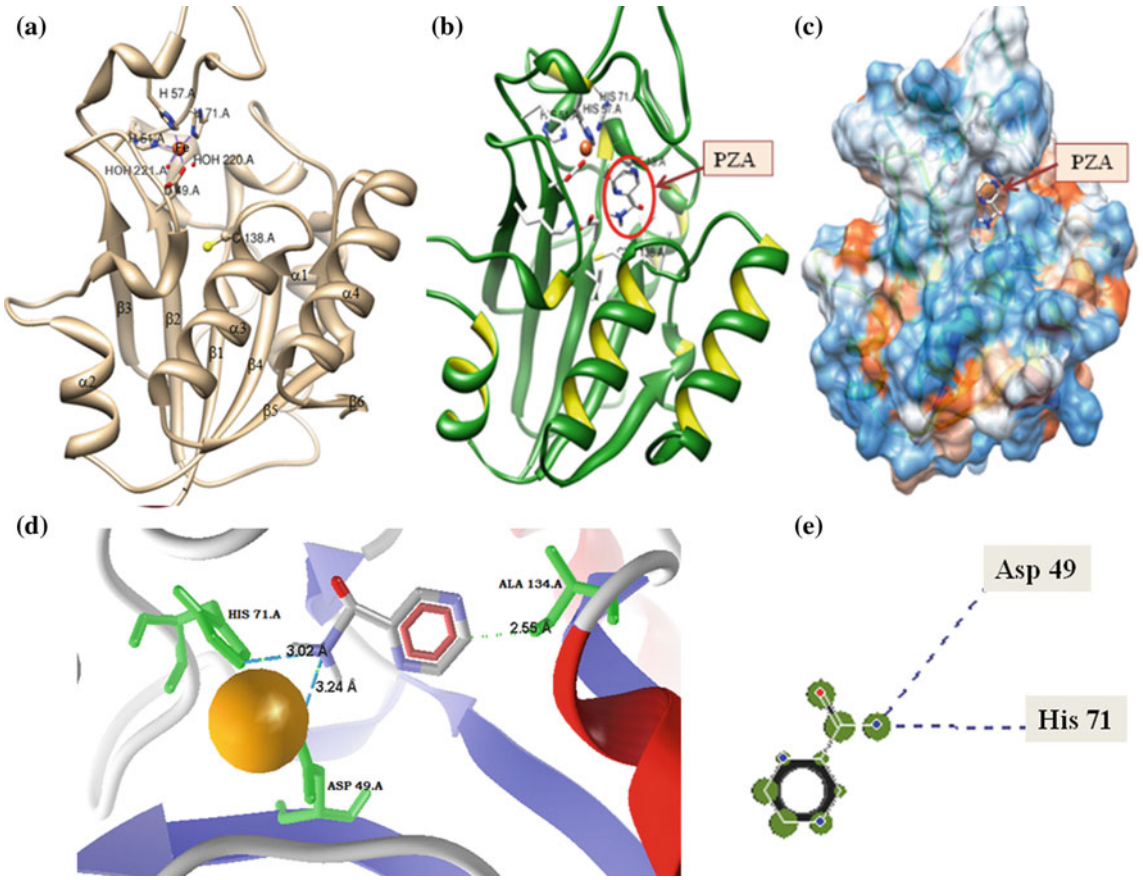

Fig. 10 **a** The optimized structure of pncA protein depicting the active binding residues and the Fe^{2+} cofactor, **b** docked conformation of bare PZA drug within the active binding site of pncA protein (PZA drug is denoted within the *red circle*), and **c** hydrophobic surface of PZA drug docked within pncA protein, **d** hydrogen bond interaction between PZA and HIS71 and ASP49 (*lines* shown in *blue*) and non-bonded interaction between PZA and Ala134 (*lines* shown in *green*) of the pncA protein. The Fe^{+2} co-factor is depicted in *orange circle*, **e** depiction of the hydrogen bonded interaction between PZA/Asp49 and PZA/His71 residues

line). The MolDock score corresponding to the binding energy of PZA and the re-rank scores are given in Table 3. We docked the sidewall functionalized PZA/(*n*,0) SWNT (both long and short nanotubes) onto pncA and sorted out the best docked pose (conformation) for binding using the re-rank score values, which are summarized in Table 3. Bare PZA drug in absence of SWCNT demonstrates a MolDock score of −54.644 au and re-rank score of −46.609 au. Upon loading onto *f*SWCNT, for 3 unit cell (*n*,*0*) SWCNT, (9,0) SWCNT gives much better docking values compared to the other nanotubes (Table 3). However, for $n = 10$, 11 and 12 the energies are quite

Table 3 Best docking poses of bare PZA and PZA functionalized onto SWCNTs into the binding site of PncA protein using MVD, based on MolDock score, re-rank score and H-bonding distance between PZA and Cys138 residue

Molecule	MolDock score	Re-rank score	H-bonding distance
PZA	−54.644	−46.609	2.992
PZA/(9,0) SWCNT 3unit cells (sidewall)	−241.496	−54.202	3.060
PZA/(9,0) SWCNT 5unit cells (sidewall)	−271.245	26.622	2.893
PZA/(9,0) SWCNT (edge)	−256.805	47.269	3.373
PZA/(10,0) SWCNT 3 unit cells (sidewall)	−223.101	−40.44	3.011
PZA/(10,0) SWCNT 5 unit cells (sidewall)	−293.068	42.999	3.066
PZA/(10,0) SWCNT (edge)	−192.143	92.526	4.772
PZA/(11,0) SWCNT 3 unit cells (sidewall)	−228.623	−21.710	3.320
PZA/(11,0) SWCNT 5 unit cells (sidewall)	−292.066	48.613	2.921
PZA/(11,0) SWCNT (edge)	−246.070	52.962	4.712
PZA/(12,0) SWCNT 3 unit cells (sidewall)	−226.527	−21.788	3.550

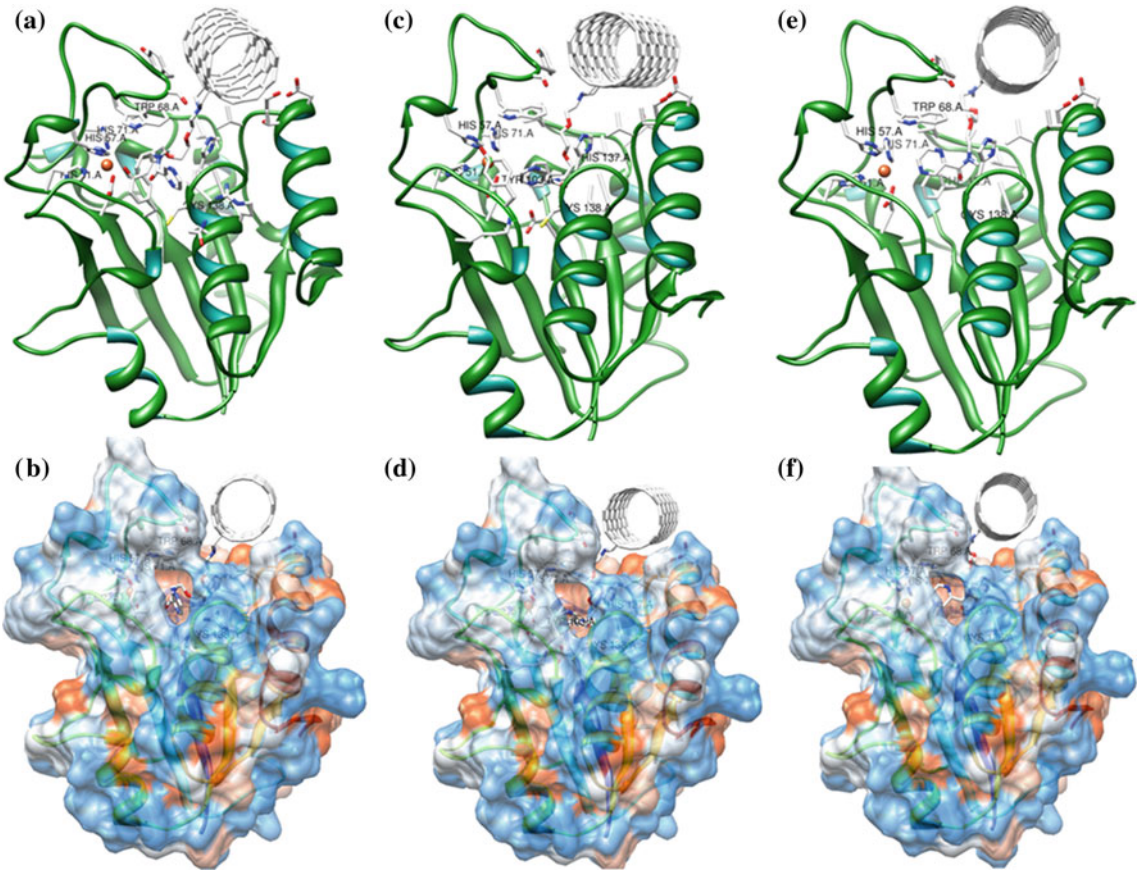

Fig. 11 **a** The docked conformation of sidewall functionalized PZA/(9,0) SWCNT comprising of 3 unit cells of SWCNT within the active binding site of pncA protein, **b** hydrophobic surface of PZA/(9,0) SWCNT docked within pncA protein, **c** docked conformation of functionalized PZA/(9,0) SWCNT comprising of 5 unit cells of SWCNT within the active binding site of pncA protein, **d** hydrophobic surface of PZA/(9,0) SWCNT docked within pncA protein, **e** docked conformation of edge functionalized PZA/(9,0) SWCNT comprising of 5 unit cells of SWCNT within the active binding site of pncA protein, **f** the hydrophobic surface of PZA/(9,0) SWCNT docked within pncA protein

comparable and the re-rank score follows the order: PZA/(9,0) SWCNT > PZA/(10,0) SWCNT > PZA/(12,0) SWCNT > PZA/(11,0) SWNT. Thus compared to bare PZA drug, nanotube loaded PZA gives much better docking energy values and nanotubes with narrow diameters are preferred for better binding with the protein compared to tubes with larger diameters, which is in good agreement with the trend in B.E. values calculated using DFT. Moving to sidewall functionalized 5 unit cell PZA/SWCNT system, we observe that with increase in the length of nanotube, the re-rank score value increases and (9,0) SWCNT gives the best docking result, which suggests that length of the nanotube as well as chirality plays an important role with nanotubes having narrow diameter more preferred for binding with the protein. The secondary structure and electrostatic surface for PZA/(9,0) SWCNT are shown in Fig. 11a, b for the sidewall functionalization (3 unit cells), Fig. 11c, d for the 5 unit cell PZA/(9,0) SWCNT and for the edge functionalization, secondary structures and electrostatic plots are shown in Fig. 11e, f, respectively. Since the mode of docking for the other studied nanotube systems are similar to (9,0) SWCNT system we have depicted the docked conformations for PZA/(9,0) SWCNT system and for the rest of the nanotube systems the docked conformation along with the secondary structures are provided in the Supporting Information, Figure S12 (3unit cells (n,0) SWCNTs for n = 10, 11 and 12) and Figure S13 (5 unit cell (n,0) SWCNTs corresponding to sidewall and edge functionalization for n = 10 and 11). The narrow diameter nanotubes are better docked compared to large diameter nanotubes as nanotubes with small diameters can easily transfuse within the body occupying a low surface volume and for intracellular transport narrow diameter nanotubes are more appropriate. On the other hand, for edge functionalized (*n*,0) SWCNTs, the re-rank score values are higher compared to sidewall functionalized PZA/(*n*,0) SWCNT systems which is in good agreement with our DFT calculations. Thus sidewall functionalized SWNTs are better docked compared to edge functionalized nanotubes onto pncA protein, and length of the PEG chain considered

in our study is quite adequate to facilitate the targeted mediation of conjugated PZA drug onto *f*SWCNT within the active binding site of pncA protein.

Docking simulation on encapsulated PZA inside SWCNTs. In addition, the docking simulations for encapsulation of single and multiple PZA molecules within SWCNTs have been investigated as encapsulation renders significant stability to the drug molecule and prevents the premature degradation before reaching the target site during administration within the body. For single PZA molecule encapsulated inside (*n*,0) SWCNTs, (10,0) SWCNT yields a much better MolDock energy value for PZA and it follows the trend:

$$\mathrm{PZA}/(10,0)\,\mathrm{SWNT} > \mathrm{PZA}/(11,0)\,\mathrm{SWNT} > \mathrm{PZA}/(12,0)\,\mathrm{SWNT}\,(\mathrm{Re-rank\,scores})$$

Compared to bare PZA drug, encapsulated PZA inside SWCNT has a much higher energy value which suggests that the presence of SWCNT helps in stabilizing PZA drug thereby sustaining its physiological activity and properties. Moving to long nanotubes, wherein multiple encapsulation of PZA molecule was carried out, 2PZA/(10,0) SWCNT yields a better MolDock energy and re-rank score values compared to 2PZA/(6,6) SWCNT (Supporting information, Figure S14e, f). In general we can state that for encapsulated PZA/(n,0) SWCNTs, multiple encapsulation of PZA is thermodynamically favorable and as for the covalent functionalization, small diameter nanotubes are better suited for drug delivery applications than nanotubes with larger diameter and simultaneous encapsulation of multiple drug molecules are possible. Figure 12a, b portrays the best docking conformation and electrostatic surface plots of one PZA molecule encapsulated inside (10,0) SWCNT (3unit cells) and for 2PZA/(10,0) SWCNT system, the docking structure and electrostatic surface plots are shown in Fig. 12c, d. We observe that multiple drug molecules can be released within the target binding site of

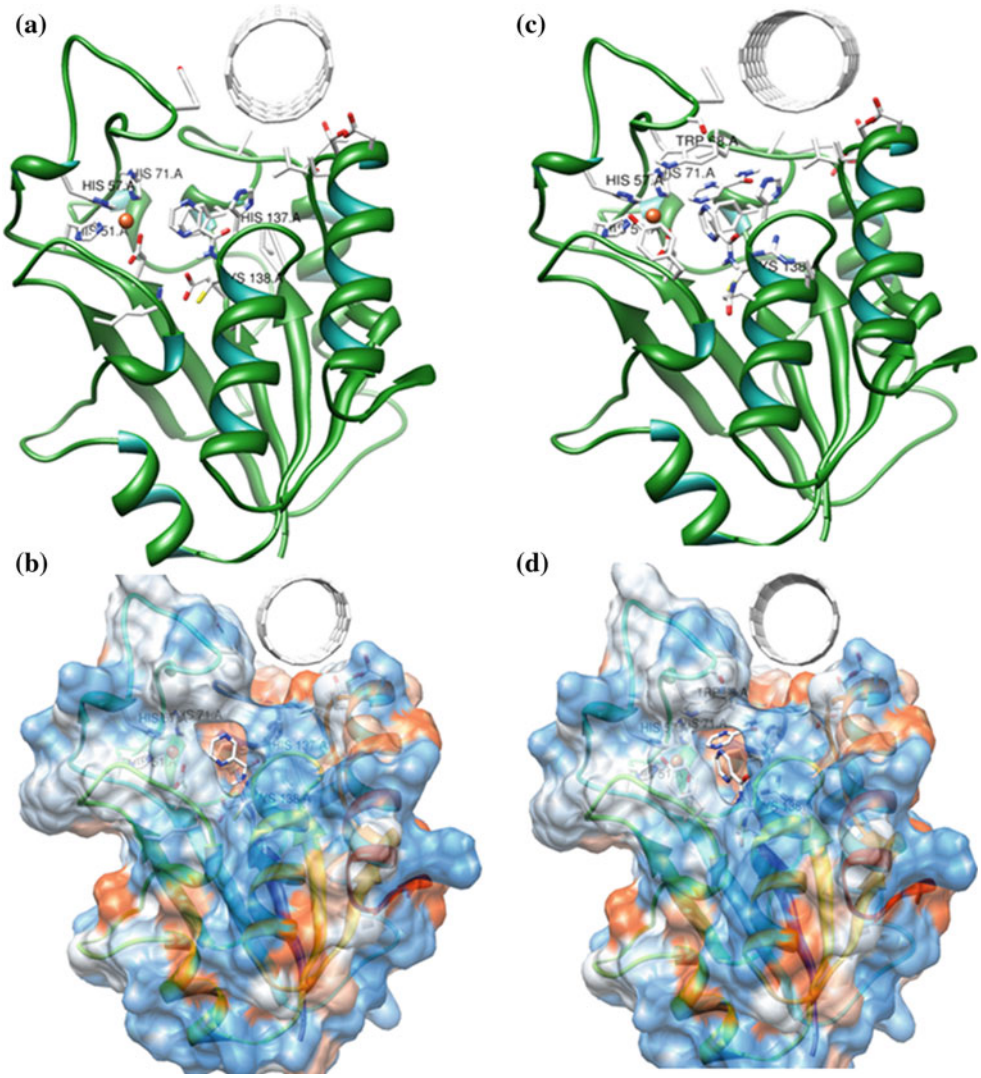

Fig. 12 **a** The docked conformation of mono PZA drug encapsulated within (10,0) SWCNT comprising of 3 unit cells of SWCNT within pncA protein, **b** hydrophobic surface of PZA/(10,0) SWCNT docked within pncA protein, **c** docked conformation of two PZA drug molecules encapsulated within (10,0) SWCNT comprising of 5 unit cells of SWCNT within the active binding site of pncA protein, **d** hydrophobic surface of PZA/(10,0) SWCNT docked within pncA protein

Table 4 Absorption, distribution, metabolism, excretion and toxicity (ADMET) analysis for bare PZA drug and PZA functionalized onto (*n*,*0*) SWCNTs

Ligand	CMC like rule	Lead like rule	Rule of 5	HIA %	C2C Permeability (nm/s)	MDCK (nm/s)	Logkp cm/h	PPB (%)	BBB c.brain/c. blood	Carcinogenicity	
										Mouse	Rat
PZA/(n,0) SWCNT for nanotubes comprising of three unit cells											
PZA/(9,0) SWCNT	Not Qualified	Violated	Violated	95.65	35.085	0.043	−5.319	90.094	10.299	−ve	+ve
PZA/(10,0) SWCNT	Not qualified	Violated	Violated	95.02	34.140	0.043	−5.031	89.235	19.202	−ve	+ve
PZA/(11,0) SWCNT	Not Qualified	Violated	Violated	95.20	35.075	0.0434	−5.031	89.397	23.066	−ve	+ve
PZA/(12,0) WSCNT	Not Qualified	Violated	Violated	95.20	35.783	0.0434	−5.031	89.419	25.671	−ve	+ve
PZA encapsulated within (*n*,*0*) and (*n*,*n*) SWCNT											
2PZA inside (10,0) SWCNT	Not Qualified	Violated	Violated	95.201	21.660	0.043	−5.031	98.947	3.768	+ve	−ve
1PZA inside (10,0) SWCNT	Not Qualified	Violated	Violated	95.201	22.957	0.043	−5.031	100	2.308	+ve	−ve
PZA/(11,0) SWCNT	Not Qualified	Violated	Violated	95.201	23.431	0.043	−5.031	100	2.413	+ve	−ve
PZA/(12,0) SWCNT	Not Qualified	Violated	Violated	95.202	24.099	0.043	−5.031	100	27.805	+ve	−ve
2PZA inside (6,6) SWCNT	Not Qualified	Violated	Violated	95.201	21.573	0.043	−5.361	100	0.916	−ve	−ve
PZA/(n,0) SWCNT for nanotubes comprising of five unit cells											
PZA/(9,0) SWCNT (sidewall)	Not Qualified	Violated	Violated	95.206	36.1958	0.043	−5.365	90.237	13.963	−ve	+ve
PZA/(9,0) SWCNT (edge)	Not Qualified	Violated	Violated	95.201	24.441	0.043	−5.031	100	1.491	+ve	−ve
PZA/(10,0) SWCNT (sidewall)	Not Qualified	Violated	Violated	95.201	34.846	0.043	−5.031	100	21.791	−ve	+ve
PZA/(10,0) SWCNT (edge)	Not Qualified	Violated	Violated	95.201	25.113	0.043	−5.031	100	1.525	+ve	−ve
PZA/(11,0) SWCNT (sidewall)	Not Qualified	Violated	Violated	95.201	35.525	0.043	−5.031	100	18.722	−ve	+ve
PZA drug	Not Qualified	Violated	Suitable	87.451	16.437	119.558	−4.242	0.711	0.153	+ve	−ve

−ve = clear evidence of carcinogenic activity, +ve = no evidence of carcinogenic activity

pncA protein for active drug binding and both the drug molecules are well grooved within the target site lying in close proximity to Cys138 residue. In all the encapsulated PZA/SWCNT systems, the nanotube does not interact with the protein and so it does not bring about any structural deformation within the protein.

ADMET analysis

We performed detailed analysis on ADMET properties on the docked conformations of PZA/nanotube systems for all the studied modes of interactions (Table 4). ADMET refers to the absorption, distribution, metabolism, excretion, and toxicity properties of a molecule within an organism [67]. ADMET descriptors include models for intestinal absorption, aqueous solubility, blood brain barrier (BBB) penetration, plasma protein binding, inhibition, hepatotoxicity and ADMET descriptors can provide a comprehensive analysis of ADMET characteristics namely:

ADMET Absorption which predicts the Human Intestinal Absorption (HIA) after oral administration and reports a classification of the absorption level [68, 69]. HIA data are the sum of bioavailability and absorption evaluated from ratio of excretion or cumulative excretion in urine, bile and faeces [70]. Although some differences exist in the experimental values of the compounds, the general classification of HIA can be classified as (1) poorly absorbed compounds (0–20 %), (2) moderately absorbed compounds (20–70 %) and (3) well absorbed compounds (70–100 %) [71]. For our studied systems, the HIA % falls within the range of 95.201–95.202 and for bare PZA drug the HIA % is calculated to be 87.451. Thus PZA functionalized SWCNT systems show better propensity for absorption compared to the bare PZA administration and the presence of nanotube support facilitates in the intracellular drug absorption.

ADMET Blood Brain Barrier (BBB) which predicts the BBB penetration of a molecule, defined as the ratio of concentration of solute (compound) on the both sides of the membrane after oral administration, and reports the predicted penetration as well as a classification of penetration level. Predicting BBB penetration signifies whether the particular compound can pass across the Central Nervous System (CNS). CNS-active compounds have the potency to pass across whereas CNS-inactive compounds cannot pass across in order to avoid CNS side effects. The general criteria for CNS activity can be put as (1) CNS-active compounds (+) with BB (C_{brain}/C_{blood}) more than 1.0 and (2) CNS-inactive compounds (−) with BB (C_{brain}/C_{blood}) less than 1.0 [72]. The CNS activity is further classified as (1) high absorption to CNS with BB (C_{brain}/C_{blood}) more than 2.0, (2) middle absorption to CNS with BB (C_{brain}/C_{blood}) 2.0–0.1 and (3) low absorption to CNS with BB (C_{brain}/C_{blood}) less than 0.1. The ADMET analysis on our studied systems shows that all the compounds except bare PZA drug are CNS-active with considerably higher CNS absorption (Table 4). Edge functionalized and PZA encapsulated SWCNT systems exhibit much lower BBB values compared to sidewall functionalized PZA/SWCNT systems which signify that edge functionalized PZA/SWCNT have mid adsorption to the CNS whereas encapsulated and sidewall functionalized systems have high adsorption to CNS.

ADMET Caco2 cell (C2C) permeability which possess multiple drug transport pathways through the intestinal epithelium. The general categories for Caco2 cell permeability can be categorized as (1) low permeability with $P_{Caco\text{-}2}$ (nm/s) less than 4, (2) middle permeability with $P_{Caco\text{-}2}$ (nm/s) around 4–70 and (3) high permeability with $P_{Caco\text{-}2}$ (nm/s) more than 70 [73]. Higher Caco-2 cell permeability predicts good human oral bioavailability. The ADMET Caco-2 cell permeability analysis on PZA functionalized SWCNTs exhibit significantly higher Caco-2 cell permeability values compared to bare PZA molecule which falls within the range of 21.573–36.196 (middle permeability) as given in Table 4. The 5 unit cell nanotubes exhibit higher Caco-2 cell permeability values compared to the 3 unit cell counterparts which indicate that longer nanotubes with narrow diameter e.g. (9,0) SWCNT demonstrate higher cell permeability across the epithelium. However, the sidewall functionalized nanotubes exhibit higher permeability compared to edge functionalization illustrating the fact that sidewall functionalization is the favored mode for drug loading and delivery within the body which is in good agreement with the thermodynamic stability obtained from the DFT calculations.

ADMET Plasma Protein Binding (PPB) which predicts whether or not a compound is likely to be get highly bound to carrier proteins in the blood. Predictions are based on the similarity between the candidate molecule and two sets of marker molecules; one used to flag binding at a level of 90 % or higher and the other at 95 % or higher. Binding levels predicted by the marker similarities are modified according to the conditions on calculated logP values. The general categories for PPB can be put as (1) chemicals strongly bound with PPB more than 90 % and (2) chemicals weakly bound with PPB less than 90 %. From the ADMET analysis we find that most of the compounds except bare PZA demonstrate very high PPB values suggesting that the nanotube-drug conjugated system shows the potency to strongly bind with the carrier proteins and in turn facilitate in the drug mediation within the body.

Thus the ADMET predictions show that presence of the SWCNT support facilitates in the enhanced adsorption of PZA drug with high plasma protein binding and higher cell permeability within the body.

Conclusions

In summary we have investigated using DFT formalism the structural stability and electronic properties of pristine zigzag (n,0) SWCNT ($n = 9$, 10, 11, and12) and functionalized nanotubes with PZA antitubercular drug molecule. The results from our study demonstrate that covalent functionalization of nanotube sidewall is thermodynamically favorable as observed from the negative binding energy values. The decrease in binding energies of PZA/(n,0) SWCNT with increasing diameter illustrates that curvature of nanotube sidewall plays an important role in determining the reactivity and nanotubes with narrow diameter are thermodynamically more favorable during the course of drug delivery. The HOMO orbitals have contribution from edge carbon atoms except in (9,0) SWCNT wherein it is delocalized along the nanotube sidewall. The charge delocalization of frontier orbitals along the tube edges show that organic moieties like carboxylic and other functional groups can be attached at the reactive nanotube ends to enhance its solubility and dispersability in biological environments of our body. In addition, a detailed analysis on the contribution of HOMO, LUMO, HOMO − n and LUMO + n orbitals provide valuable insight and significant implications towards the orbital distribution in pristine and functionalized SWCNT systems. The functionalization of zigzag (n,0) SWCNTs cause perturbation in the electronic structure and properties of CNT and the frontier orbitals are modified compared to pristine nanotube. DFT findings supported by docking simulations suggest that SWCNTs facilitate in the effective and target specific delivery of PZA drug within the active binding cavity of pncA protein and narrow diameter nanotubes are well docked with the protein rather than tubes with larger diameters and length of PEG chain is reasonably adequate for the delivery of PZA drug within the specific active binding site of pncA protein. Furthermore, encapsulation facilitates in the multiple loading and delivery of PZA molecules within the protein and for all the studied nanosystems conjugated with PZA molecule SWCNT does not bring about any conformational change within the protein. ADMET analysis provide a generalized understanding towards the efficacy of incorporating SWCNTs for the functionalization of PZA drug and its activity profile compared to administration of bare PZA drug. Hence from our theoretical study we can conclude that SWCNTs can behave as efficient nanovectors for loading of PZA antitubercular drug onto its sidewall and covalent functionalization via sidewall and edge attachment of functional units helps in achieving this goal, but the long term objective remains to better understand the mediation and subsequent release of therapeutics from *f*SWNT at the target specific cells especially at the experimental level of study, to make this area of research more promising in the near future applications.

Acknowledgments This work is supported by the funding from the Department of Science and Technology (DST), New Delhi, India.

References

1. Reich S, Thomsen C, Maultzsch J (2004) Carbon nanotubes: basic concepts and physical properties. Wiley-VCH, Weinheim 215
2. Challa SS, Kumar R, Hormes J, Leuschner C (2005) Nanofabrication towards biomedical applications, techniques, tools, applications and impact. Wiley-VCH, Weinheim, pp 236–289
3. Ferrari M (2005) Cancer nanotechnology: opportunities and challenges. Nat Rev Cancer 5(3):161–171
4. Kam NWS, Liu Z, Dai H (2006) Carbon nanotubes as intracellular transporters for proteins and DNA: an investigation of the uptake mechanism and pathway. Angew Chem Int Ed 45:577–581
5. Liu Y, Wu D-C, Zhang W-D, Jiang X, He C-B, Chung TS, Goh SH, Leong KW (2005) Polyethylenimine-grafted multiwalled carbon nanotubes for secure noncovalent immobilization and efficient delivery of DNA. Angew Chem Int Ed 44(30): 4782–4785
6. Dhar S, Liu Z, Thomale J, Dai H, Lippard SJ (2008) Targeted single-wall carbon nanotube-mediated Pt(IV) prodrug delivery using folate as a homing device. J Am Chem Soc 130(34): 11467–11476
7. Kam NWS, Liu Z, Dai H (2005) Functionalization of carbon nanotubes via cleavable disulfide bonds for efficient intracellular delivery of siRNA and potent gene silencing. J Am Chem Soc 127(36):12492–12493
8. Smith DA, van de Waterbeemd H (1999) Pharmacokinetics and metabolism in early drug discovery. Curr Opin Chem Biol 3(4):373–378
9. Besteman K, Lee JO, Wiertz FGM, Herring HA, Dekker C (2003) Enzyme-coated carbon nanotubes as single-molecule biosensors. Nano Lett 3(6):727–730
10. Chen X, Tam UC, Czlapinski JL, Lee GS, Rabuka D, Zettl A, Bertozzi CR (2006) Interfacing carbon nanotubes with living cells. J Am Chem Soc 128(19):6292–6293
11. Kang Y, Wang Q, Liu YC, Shen JW, Wu T (2010) Diameter selectivity of protein encapsulation in carbon nanotubes. J Phys Chem B 114(8):2869–2875
12. Bianco A, Kostarelos K, Partidos CD, Prato M (2005) Biomedical applications of functionalised carbon nanotubes. M Chem Commun 5:571–577
13. Lacerda L, Bianco A, Prato M, Kostarelos K (2006) Carbon nanotubes as nanomedicines: from toxicology to pharmacology. Adv Drug Del Rev 58(14):1460–1470
14. Bianco A, Hoebeke J, Godefroy S, Chaloin O, Pantarotto D, Briand JP, Muller S, Prato CD (2005) Cationic carbon nanotubes bind to CpG oligodeoxynucleotides and enhance their immunostimulatory properties. J Am Chem Soc 127(1):58–59

15. Chełmecka E, Pasterny K, Kupka T, Stobiński L (2012) DFT studies of COOH tip-functionalized zigzag and armchair single wall carbon nanotubes. J Mol Model 18(5):2241–2246
16. Wu W, Wieckowski S, Pastorin G, Benincasa M, Klumpp C, Briand J-P, Gennaro R, Prato M, Bianco A (2005) Targeted delivery of amphotericin B to cells by using functionalized carbon nanotubes. Angew Chem Int Ed 44(39):6358–6362
17. Liu Z, Sun X, Nakayama-Ratchford N, Dai H (2007) Supramolecular chemistry on water-soluble carbon nanotubes for drug loading and delivery. ACS Nano 1(1):50–57
18. Bianco A, Kostarelos K, Partidos CD, Prato M (2005) Biomedical applications of functionalised carbon nanotubes. Chem Commun 5:571–577
19. Sahoo NG, Bao H, Pan Y, Pal M, Kakran M, Cheng HKF, Li L, Tan LP (2011) Functionalized carbon nanomaterials as nanocarriers for loading and delivery of a poorly water-soluble anticancer drug: a comparative study. Chem Commun 47(18): 5235–5237
20. Nimmagadda A, Thurston K, Nollert MU, McFetridge PS (2006) Chemical modification of SWNT alters in vitro cell-SWNT interactions. J Biomed Mater Res Part A 76A:614–625
21. Murugesan S, Park TJ, Yang H, Mousa S, Linhardt RJ (2006) Blood compatible carbon nanotubes-nano-based neoproteoglycans. Langmuir 22(8):3461–3463
22. Zhang L, Xia J, Zhao Q, Liu L, Zhang Z (2010) Functional graphene oxide as a nanocarrier for controlled loading and targeted delivery of mixed anticancer drugs. Small 6(4):537–544
23. Wu W, Li R, Bian X, Zhu Z, Ding D, Li X, Jia Z, Jiang X, Hu Y (2009) Covalently combining carbon nanotubes with anticancer agent: preparation and antitumor activity. ACS Nano 3(9):2740–2750
24. Saikia N, Deka RC (2011) Density functional calculations on adsorption of 2-methylheptylisonicotinate antitubercular drug onto functionalized carbon nanotube. Comput Theor Chem 964:257–261
25. Saikia N, Pati SK, Deka RC (2012) First principles calculation on the structure and electronic properties of BNNTs functionalized with isoniazid drug molecule. Appl Nanosci. doi:10.1007/s13204-012-0124-6
26. Murakami T, Fan J, Yudasaka M, Iijima S, Shiba K (2006) Solubilization of single-wall carbon nanohorns using a PEG-doxorubicin conjugate. Mol Pharm 3(4):407–414
27. Popov AM, Lozovik YE, Fiorito S, Yahia L (2007) Biocompatibility and applications of carbon nanotubes in medical nanorobots. Int J Nanomed 2:361–372
28. Sung J, Barone PW, Kong H, Strano MS (2009) Sequential delivery of dexamethasone and VEGF to control local tissue response for carbon nanotube fluorescence based micro-capillary implantable sensors. Biomaterials 30(4):622–631
29. Ali-Boucetta H, Al-Jamal KT, McCarthy D, Prato M, Bianco A, Kostarelos K (2008) Multiwalled carbon nanotube-doxorubicin supramolecular complexes for cancer therapeutics. Chem Commun 4:459–461
30. Pastorin G, Wu W, Wieckowski S, Briand JP, Kostarelos K, Prato M, Bianco A (2006) Double functionalisation of carbon nanotubes for multimodal drug delivery. Chem Commun 21:1182–1184
31. Zanella I, Fagan SB, Mota R, Fazzio A (2007) Ab initio study of pristine and Si-doped capped carbon nanotubes interacting with nimesulide molecules. Chem Phys Lett 439:348–353
32. Liu Z, Winters M, Holodniy M, Dai H (2007) siRNA delivery into human T cells and primary cells with carbon-nanotube transporters. Angew Chem Int Ed 46(12):2023–2027
33. Zerda ADL, Zavaleta C, Keren S, Vaithilingam S, Bodapati S, Liu Z, Levi J, Smith BR, Ma TJ, Oralkan O, Cheng Z, Chen X, Dai H, Khuri-Yakub BT, Gambhir SS (2008) Carbon nanotubes as photoacoustic molecular imaging agents in living mice. Nat Nanotechnol 3(9):557–562
34. Liu Z, Cai W, He L, Nakayama N, Chen K, Sun X, Chen X, Dai H (2007) In vivo biodistribution and highly efficient tumour targeting of carbon nanotubes in mice. Nat Nanotechnol 2(1):47–52
35. Cole ST, Eisenach KD, McMurray DN, Jacobs WR Jr (eds) (2005) Tuberculosis and the tubercle bacillus. ASM Press, Washington
36. Maher D, Chaulet P, Spinaci S, Harries A (1997) Treatment of tuberculosis: guidelines for national programmes. Wold Health Organization, Geneva
37. Petrella S, Gelus-Zietal N, Maudry A, Laurans C, Boudjelloul R, Sougakoff W (2011) Crystal structure of the pyrazinamidase of *Mycobacterium tuberculosis*: insights into natural and acquired resistance to pyrazinamide. PLoS ONE 6:e15785. doi:10.1371/journal.pone.0015785
38. Konno K, Feldmann FM, McDermott W (1967) Pyrazinamide susceptibility and amidase activity of tubercle bacilli. Am Rev Respipr Dis 95(3):461–469
39. Scorpio A, Zhang Y (1996) Mutations in pncA, a gene encoding pyrazinamidase/nicotinamidase, cause resistance to the antituberculous drug pyrazinamide in tubercle bacillus. Nat Med 2(6):662–667
40. Sheen P, Ferrer P, Gilman RH, Llano JL, Fuentes P, Valencia E, Zimic MJ (2009) Effect of pyrazinamidase activity on pyrazinamide resistance in *Mycobacterium tuberculosis*. Tuberculosis 89(2):109–113
41. Du X, Wang W, Kim R, Yakota H, Nguyen H, Kim SH (2001) Crystal structure and mechanism of catalysis of a pyrazinamidase from *Pyrococcus horikoshii*. Biochem 40(47):14166–14172
42. Lemaitre N, Callebaut I, Frenois F, Jarlier V, Sougakoff W (2001) Study of the structure-activity relationships for the pyrazinamidase (*PncA*) from *Mycobacterium tuberculosis*. Biochem J 353:453–458
43. Gallo M, Favila A, Glossman-Mitnik D (2007) DFT studies of functionalized carbon nanotubes and fullerenes as nanovectors for drug delivery of antitubercular compounds. Chem Phys Lett 447(1–3):105–109
44. Saikia N, Deka RC (2010) Theoretical study on pyrazinamide adsorption onto covalently functionalized (5,5) metallic single-walled carbon nanotube. Chem Phys Lett 500(1–3):65–70
45. Saikia N, Deka RC (2012) A comparison of the effect of nanotube chirality and electronic properties on the π–π interaction of single-wall carbon nanotubes with pyrazinamide antitubercular drug. Int J Quant Chem. doi:10.1002/qua.24275
46. Georgakilas V, Kordatos K, Prato M, Guldi DM, Holzinger M, Hirsch A (2002) Organic functionalization of carbon nanotubes. J Am Chem Soc 124(5):760–761
47. Lu X, Tian F, Xu X, Wang N, Zhang Q (2003) Theoretical exploration of the 1,3-dipolar cycloadditions onto the sidewalls of (*n*, *n*) armchair single-wall carbon nanotubes. J Am Chem Soc 125(34):10459–10464
48. Yao Z, Braidy N, Botton GA, Adronov A (2003) Polymerization from the surface of single-walled carbon nanotubes-preparation and characterization of nanocomposites. J Am Chem Soc 125(51):16015–16024
49. Hirsch A, Vostrowsky O (2005) Functionalization of carbon nanotubes. Top Curr Chem 245:193–237
50. Delley B (1990) An all-electron numerical method for solving the local density functional for polyatomic molecules. J Chem Phys 92:508–517
51. Perdew JP, Wang Y (1992) Accurate and simple analytic representation of the electron-gas correlation energy. Phys Rev B 45:13244–13249

52. Pauling L (1960) The nature of chemical bond. Cornell University Press, Ithaca
53. Pearson RG (1963) Hard and soft acids and bases. J Am Chem Soc 85:3533–3539
54. Pearson RG (1997) Chemical hardness: applications from molecules to solids. Wiley-VCH GMBH, Weinheim
55. Mulliken RS (1934) Electronic structures of molecules. XI. Electroaffinity, molecular orbitals and dipole moments. J Chem Phys 2:782–793
56. Seal A, Aykkal R, Babu RO, Ghosh M (2011) Docking study of HIV-1 reverse transcriptase with phytochemicals. Bioinformation 5(10):430–439
57. Thomsen R, Christensen MH (2006) MolDock: a new technique for high-accuracy molecular docking. J Med Chem 49(11): 3315–3321
58. Storn R, Price K (1995) Differential evolution—a simple and efficient adaptive scheme for global optimization over continuous spaces; technical report. International Computer Science Institute, Berkley
59. Yang JM, Chen CC (2004) GEMDOCK: a generic evolutionary method for molecular docking. Proteins 55(2):288–304
60. Morris GM, Goodsell DS, Halliday RS, Huey R, Hart WE, Belew RK, Olson AJ (1998) Automated docking using a Lamarckian genetic algorithm and an empirical binding free energy function. J Comput Chem 19(14):1639–1662
61. Lu X, Tian F, Xu X, Wang N, Zhang Q (2003) A theoretical exploration of the 1,3-dipolar cycloadditions onto the sidewalls of (n, n) armchair single-wall carbon nanotubes. J Am Chem Soc 125(34):10459–10464
62. Girifalco LA, Hodak M (2002) Van der Waals binding energies in graphitic structures. Phys Rev B 65(125404):1–5
63. Borstnik U, Hodoscek M, Janezic D, Lukovits I (2005) Electronic structure properties of carbon nanotubes obtained by density functional calculations. Chem Phys Lett 411(4–6):384–388
64. Unissa AN, Selvakumar N, Hassan S (2009) Insight to pyrazinamide resistance in *Mycobacterium tuberculosis* by molecular docking. Bioinformation 4(1):24–29
65. Scorpio A, Zhang Y (1996) Mutations in *pncA*, a gene encoding pyrazinamidase/nicotinamidase, cause resistance to the antituberculous drug pyrazinamide in tubercle bacillus. Nat Med 2:662–667
66. Zhang H, Deng JY, Bi LJ, Zhou YF, Zhang ZP, Zhang CG, Zhang Y, Zhang XE (2008) Characterization of *Mycobacterium tuberculosis* nicotinamidase/pyrazinamidase. FEBS J 275(4): 753–762
67. Prentis RA, Lis Y, Walker SR (1988) Pharmaceutical innovation by the seven UK-owned pharmaceutical companies (1964–1985). Br J Clin Pharmac 25(3):387–396
68. Egan WJ, Merz KM Jr, Baldwin JJ (2000) Prediction of drug absorption using multivariate statistics. J Med Chem 43(21): 3867–3877
69. Ghose AK, Viswanadhan VN, Wendoloski JJ (1998) Prediction of hydrophobic (Lipophilic) properties of small organic molecules using fragmental methods: an analysis of ALOGP and CLOGP methods. J Phys Chem 102:3762–3770
70. Zhao YH, Le J, Abraham MH, Hersey A, Eddershaw PJ, Luscombe CN, Boutina D, Beck G, Sherborne B, Cooper I, Platts JA (2001) Evaluation of human intestinal absorption data and subsequent derivation of a quantitative structure-activity relationship (QSAR) with the Abraham descriptors. J Pharm Sci 90(6): 749–784
71. Yee S (1997) In vitro permeability across Caco-2 cells (Colonic) can predict in vivo (small intestinal) absorption in man—fact or myth. Pharm Res 14(6):763–766
72. Bemis GW, Murcko MA (1992) Designing libraries with CNS activity. J Med Chem 42(24):4942–4951
73. Yazdanian M, Glynn SL, Wright JL, Hawi A (1998) Correlating partitioning and Caco-2 cell permeability of structurally diverse small molecular weight compounds. Pharm Res 15(9):1490–1494